Journal of Materials Chemistry A

Accepted Manuscript

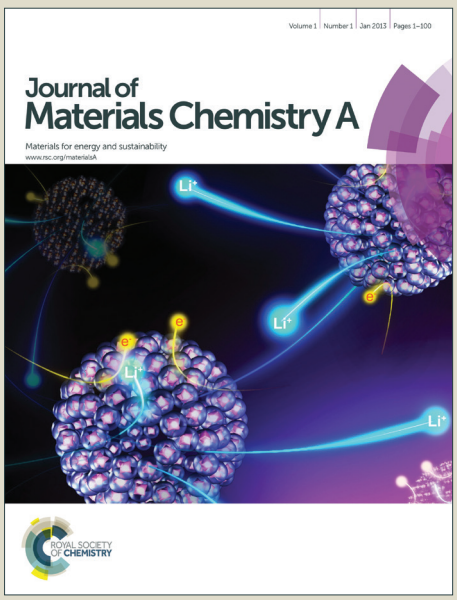

ROYAL SOCIETY OF CHEMISTRY

www.rsc.org/materialsA

Direct growth of $FePO_4$/reduced graphene oxide nanosheet composite for sodium-ion battery

Yao Liu,[a] Shuojiong Xu,[a] Shiming Zhang,[ab] Junxi Zhang,[*a] Jinchen Fan,[a] Yirong Zhou.[a]

[a] *Shanghai Key Laboratory of Materials Protection and Advanced Materials in Electric Power, Shanghai University of Electric Power, Shanghai, 200090, People's Republic of China.*

[b] *State Key Laboratory of Silicon Materials, Key Laboratory of Advanced Materials and Applications for Batteries of Zhejiang Province & Department of Materials Science and Engineering, Zhejiang University, Hangzhou 310027, People's Republic of China.*

* Corresponding author. Tel. /Fax. : +86-21-35303677.

E-mail address: zhangjunxi@shiep.edu.cn.

Abstract: In this article, an $FePO_4$/reduced graphene oxide (rGO) nanosheet has been synthesized through a micro-emulsion technique, and exhibits excellent electrochemical performance in discharging specific capacity and rate capability. The $FePO_4$ nanospheres grow on both sides of the rGO in a single layer by means of a non-covalent bond. The first discharge-specific capacity of this cathode material is up to 130.5 mAh g^{-1} and remains at 153.4 mAh g^{-1} after the 70th cycle at 0.1C. The discharge-specific capacity of $FePO_4$/rGO is maintained at 154.5 mAh g^{-1}, 151.6 mAh g^{-1}, 122.3 mAh g^{-1} and 100.6 mAh g^{-1}, at 0.1C, 0.2C, 0.5C and 1C, respectively. The result indicates that the $FePO_4$/rGO nanosheet composition has great potential as a cathode material for a sodium-ion battery.

Keywords: Non-covalent bond; Iron phosphate; Reduced graphene oxide; Micro-emulsion; Sodium-ion battery.

1. Introduction

Recently, with an emphasis on environmental protection and reducing fossil fuel consumption, lithium ion batteries (LIBs)[1, 2] have been considered as the most promising energy system for application in electric vehicles and stationary energy storage.[3-5] However, lithium is not an abundant resource in the earth's crust and lithium is not evenly distributed around the world. The increasing price of the raw material will certainly bring rising costs of the batteries with the large-scale application of LIBs.[6-9] For these reasons, it is important to find abundant resources and cheap raw materials for rechargeable batteries. Sodium is located below lithium in the periodic table, and both show similar chemical properties in many respects.[10] LIBs and sodium-ion batteries (SIBs) have the same fundamental principle for the alkali-ion shuttle back and forth between the two electrodes during the process of charging and discharging. Moreover, the abundant, inexpensive alkali element sodium is considered as a suitable alternative for lithium in large-scale stationary energy storage, in relation to renewable energy and smart grids.[7, 11] Most importantly, it may also be a challenge to find an ideal cathode material for SIBs because most LIB cathode materials are not suitable, because the radius of sodium ions is larger than that of lithium ions.[8, 10, 12-15]

Among the different kinds of cathode materials, much attention has been given to olivine lithium iron phosphate as a suitable candidate since it was first reported by Padhi et al.[16] This is mainly because of its many advantages, such as excellent cycling performance, low cost, environmentally friendly properties, high theoretical capacity

(170 mAh g^{-1}), high-voltage plateau and safety.[17-19] For $LiFePO_4$ deintercalated 1 molar lithium ion per formula unit during the charging process, corresponding to the phase transformation from $LiFePO_4$ phase to $FePO_4$ phase, both maintain a similar structure.[17] Therefore, it is feasible for $FePO_4$ to be used as a cathode material, as it has more advantages. Firstly, ferric iron (Fe^{3+}) compounds are inexpensive and easily available raw materials. Moreover, the synthesis process of $FePO_4$ is simple, environmentally friendly, and does not require a protective atmosphere and higher theoretical capacity (178 mAh g^{-1}).[20] However, as a cathode material for rechargeable batteries it has inherent disadvantages, such as low electronic conductivity and poor ionic conductivity. To overcome these shortcomings, cation doping is usually an effective method to improve the electronic and ionic conductivity.[21, 22] Unfortunately, carbon coating is not suitable to improve the electrochemical performance of $FePO_4$ because of easy reduction from Fe^{3+} to Fe^{2+} when adding carbon sources under 460°C heat treatment.[23, 24]

Since graphene was first prepared by mechanical exfoliation and chemical vapour deposition, this material has attracted huge interest, owing to its large surface area, high electronic conductivity and excellent chemical stability.[25-29] Hyun Ae Cha et al. used nitrogen-doped open pore channelled graphene with TiO_2 nanoparticles as anode material for SIB and obtained excellent electrochemical performance.[30] Jiao et al. reported on the preparation of a graphene-like MoS_2/graphene nanocomposite by hydrolysis of lithiated MoS_2 ($LiMoS_2$) as the anode material for LIB.[31] Wang et al. made NiS nanorod-assembled nanoflowers grow on graphene to fabricate composites

for lithium-ion storage application that exhibit high capacity and a good high-rate capability.[32] Fan et al. used rhodanineacetic acid-pyrene (RAAP) to functionalize the graphene, to make $FePO_4$ particles grow on it in order to fabricate $FePO_4$/graphene nanosheet composite for LIBs.[33, 34] However, this process of synthesis is very complicated and the electrochemical performance was not satisfactory. Xu et al. used non-covalent bonds to fabricate maize-like $FePO_4$/MCNT core-shell nanowire composites as the cathode material for SIBs.[24] However, direct growth of $FePO_4$/rGO nanosheet composite for SIBs by non-covalent bonds in a micro-emulsion system has not yet been reported.

Herein, firstly, the as-prepared rGO was dispersed by ultrasound in a micro-emulsion system. Fortunately, rGO disperses well in an oil solvent.[35, 36] Subsequently, amorphous $FePO_4$ nanospheres were loaded uniformly onto the rGO to obtain an $FePO_4$/rGO nanosheet composition. This composition acts as the cathode material for SIBs, with the first discharge-specific capacity as high as 130.5 mAh g^{-1}, and remaining at 153.4 mAh g^{-1} after the 70th cycle at 0.1C. The discharge-specific capacity of $FePO_4$/rGO was maintained at 154.5 mAh g^{-1}, 151.6 mAh g^{-1}, 122.3 mAh g^{-1}, and 100.6 mAh g^{-1} at 0.1C, 0.2C, 0.5C and 1C, respectively. The unique structure of the $FePO_4$/rGO nanosheet composition greatly enhances the efficient electronic and ionic conductivity, allowing a high specific capacity and high rate capability of this cathode material to be obtained.

2. Experiment

2.1 Preparation of $FePO_4$/rGO and $FePO_4$

All chemicals were analytically pure reagents without further purification. Firstly, flake graphite was used to prepare rGO by Hummers' method.[29, 37, 38] The synthesis process of the $FePO_4$/rGO composite by a micro-emulsion technique is illustrated in Fig. 1. 0.1 mol/L $Fe(NO_3)_3$•$9H_2O$ and 0.1 mol/L $NH_4H_2PO_4$ were prepared, respectively. Two cyclohexane/Triton X-100/n-butylalcohol micro-emulsion systems were prepared, in a volume ratio of 5:3:1, with markings A and B, respectively. 20% rGO (the mass ratio of rGO to $FePO_4$) was added to micro-emulsion A and ultrasound was applied for half an hour. Then 100 ml 0.1 mol/L $Fe(NO_3)_3$•$9H_2O$ and 0.1 mol/L $NH_4H_2PO_4$ were added to A and B, respectively, at the same time, and stirred magnetically for an hour. After that, both were transferred into a glass reaction kettle and ammonia was added dropwise to adjust the pH value to 2.6. The suspension continued to react at 45°C and pH 2.6 for 3h. After aging for 3 hours, the solution was centrifuged at 8000 r/min for 15 minutes, and washed three times with mixed alcohol and acetone (volume ratio of 1:1). Lastly, the resulting precipitates were dried at 100°C for 12 h, and then calcined in a tube furnace at 460°C for 3 h, under an N_2 atmosphere. In contrast, the pure $FePO_4$ was synthesized using the same method but without adding rGO.

2.2 Sample characterization

The crystal features of the samples were characterized by X-ray diffraction (XRD), using a Bruker D8 Advance X-ray diffractometer with Cu-Kα radiation. The diffraction angle (2θ) was from 20° to 70°, at a rate of 2°/min and step size of 0.02°. Raman spectrum measurements were carried out using a Horiba Raman spectrometer with a

514.5 nm wavelength incident laser light. The morphology and composition of the $FePO_4$/rGO was characterized by scanning electron microscopy and energy dispersive spectrometry (SEM-EDS), using the XL-30 FEG model. Transmission electron microscopy (TEM, JEM-2100; 200KeV) was used to study the microstructure of the $FePO_4$/rGO and $FePO_4$. The final content of rGO in the $FePO_4$/rGO composite was obtained on the basis of TGA (Thermogravimetry Analyzer, DTA7, Perkin Elmer) measurements. The temperature increase range was from room temperature to 800°C, at a rate of 10°C/min under air atmosphere.

2.3 Electrochemical testing

The cathode electrode material was prepared by ball-milling with the ratio of active material, conductive material and PTFE (polytetra-fluoroethylene), at 62:30:8 in weight. The typical electrode mass was 15 mg. Electrochemical performance was evaluated with a CR-2016 type coin, consisting of the cathode material and a metallic-sodium anode, with 1 mol/L $NaClO_4$ in a mixture of ethylene carbonate/dimethyl carbonate (EC/DMC, 1:1 by volume), with electrolyte and glass-fibre as separators. All coin batteries were assembled in an argon-filled glove box. Galvanostatic cycling was tested at different current densities in the range of 1.5–4.2V, using a Land CT2001A battery test system (Wuhan Land, China). Electrochemical impedance spectroscopy (EIS) and cyclic voltammetry (CV) tests were carried out on the electrochemical work station (Chenghua CHI660C, Shanghai, China) in the voltage window of 1.5–4.2V, at room temperature (25ºC). The CV scanning rate was 0.05 mV s^{-1}. The EIS perturbation signal was 5 mV, and the frequency range was from 10^{-2} Hz to

10^5 Hz.

3. Results and Discussion

Fig. 2 illustrates the powder XRD patterns of the pure $FePO_4$ and $FePO_4$/rGO compositions. Both display no obvious peak, but the $FePO_4$/rGO has a broad peak between 20° and 40° which corresponds to the rGO.[39] The structure of the $FePO_4$ nanoparticles still remains amorphous under calcining at 460°C, which agrees with previous reports.[24] The result of the XRD patterns shows that the amorphous structure of $FePO_4$ is unchanged by adding rGO. To further examine the composite structure of $FePO_4$/rGO, the Raman spectrum is provided in Fig. 3. According to the patterns, $FePO_4$/rGO and rGO show similar Raman spectra as two peaks at 1353.1 cm^{-1} and 1590.5 cm^{-1} respectively, which correspond to the D and G bonds of graphene.[40] Both show a stronger G bond than D band and the intensity ratios of the I_D/I_G were about 0.97 and 0.93, which indicate that the $FePO_4$/rGO and as-prepared rGO have a highly ordered graphene structure.[41] The similar values of I_D/I_G of $FePO_4$/rGO and as-prepared rGO prove that the structure of rGO was kept well during the synthesis process, which provides favourable conditions for the nucleation and growth of $FePO_4$ nanospheres on the rGO. Fig. 4 displays the TGA-DSC curve of the $FePO_4$/rGO. The $FePO_4$/rGO powders exhibit two steps of mass loss at about 50°C and 350°C, which correspond to the dehydration process and rGO oxidation.[42] The total weight loss is observed to be about 22.4%. The mass loss of water is about 3.3% and 19.1% of rGO, which is less than the loading weight (20%wt) of rGO, which may be due to losing some rGO during the washing process.

The scanning electron microscopy (SEM) image (Fig. 5a) shows that the as-prepared rGO by Hummers' method has typical characteristics which are consistent with those reported.[43] The SEM and TEM images of pure $FePO_4$ without adding rGO are shown in Fig. 5b and Fig. 5c, respectively, and display uniform spherical morphology, with an average diameter of about 20 nm. Fig. 5d and Fig. 5e show the SEM images of the as-prepared $FePO_4$/rGO nanosheet at different magnifications. It is obvious that the $FePO_4$ nanospheres grow uniformly on the rGO to form the nanosheet composition. In addition, the average thickness of the $FePO_4$/rGO nanosheet was estimated to be about 40 nm according to Fig. 5d, corresponding to the sum of the diameters of two $FePO_4$ nanospheres, which means that the $FePO_4$ nanospheres grow on both sides of the rGO in a single layer. To further examine the structure of the $FePO_4$/rGO nanosheet, the TEM image is provided in Fig. 5f. We can see that the $FePO_4$ nanospheres are in tight contact with the rGO, which agrees well with the result of the SEM test. In order to further prove the existence of the rGO, the selected area electron diffraction (SAED) pattern of the rGO is shown in the inset of Fig. 5f, which exhibits the typical rings of rGO.[44] The elemental analysis of the $FePO_4$ and $FePO_4$/rGO carried out by EDS is shown in Fig. 5g and Fig. 5h, Both prove that the components of $FePO_4$ and $FePO_4$/rGO as the ratio of Fe: P are near to 1:1. According to Fig. 5h, the weight percentage of the carbon is 18.82%, which is well consistent with the result of TGA as mentioned before.

The high-resolution TEM images of $FePO_4$/rGO before and after sodiation are presented in Fig. 6. The scanning TEM image of amorphous $FePO_4$ (Fig. 6a) clearly

displays no distinguishable lattice fringes. However, the image of sodiated $FePO_4$/rGO (Fig. 6b) shows obvious fringe widths with dimensions of 3.43 Å and 3.35 Å that correspond to the (020) and (201) diffraction planes, respectively, of $NaFePO_4$ (calculated from ICSD).[45] The results show that the sodium-ions insert amorphous $FePO_4$ to fabricate micro-crystalline $NaFePO_4$, which agrees well with previous work.[46]

The CV of $FePO_4$/rGO and $FePO_4$ is shown in Fig. 7, and both display a pair of current peaks located at 2.83/2.43 V and 3.03/2.24 V, respectively, corresponding to the redox of Fe^{2+}/Fe^{3+}. According to Fig. 7, the redox interval potential of $FePO_4$/rGO between two anodic/cathodic peaks is 0.4 V, and is 0.77 V for $FePO_4$. The CV result also demonstrates that the process of sodiation/desodiation is a continuous single-phase redox reaction, because both curves have broad redox peaks,[47, 48] and the $FePO_4$/rGO has a more outstanding cycle reversibility for its lower value of redox interval potential, compared with pure $FePO_4$. Also, the area of $FePO_4$/rGO CV is obviously larger than pure $FePO_4$, which agrees well with the apparent improvement in the discharge-specific capacity, as mentioned below.

The charge/discharge voltage profiles of $FePO_4$/rGO and $FePO_4$ at the 1st and 20th cycles at 0.1C are shown in Fig. 8. Both of them exhibit a monotonous voltage change without an obvious voltage platform, which agrees well with the results of the CV test. In addition, the shapes of the profiles have typical characteristics of $FePO_4$ as the cathode material for sodium-ion batteries.[22, 49, 50] The 1st and 20th cycles' discharge-specific capacities of $FePO_4$/rGO were 130.5 mAh g^{-1} and 154.6 mAh g^{-1},

respectively, and 116.6 mAh g^{-1} and 126.3 mAh g^{-1} for pure $FePO_4$. Although the discharge-specific capacity of these two materials increased after the 20th cycle, the discharge-specific capacity of $FePO_4$/rGO improved more. The galvanostatic charge/discharge profiles of $FePO_4$/rGO at the 1st, 2nd, 5th, 10th, 20th, 50th, and 70th cycles at 0.1C are shown in Fig. 9, and correspond to the discharge-specific capacities of 130.5 mAh g^{-1}, 117.8 mAh g^{-1}, 133.3 mAh g^{-1}, 149.9 mAh g^{-1},153.1 mAh g^{-1}, 151.1 mAh g^{-1} and 152.3 mAh g^{-1}, respectively.

The discharge-specific capacity profiles of $FePO_4$/rGO and $FePO_4$ at 0.1C are displayed in Fig. 10. The initial discharge capacity of $FePO_4$ is 116.6 mAh g^{-1} and remains at 115.1 mAh g^{-1} after the 70th cycle, i.e. only 64% of the theoretical capacity (178 mAh g^{-1}). As for the $FePO_4$/rGO nanosheet composition, the first discharge capacity is 130.5 mAh g^{-1} and is maintained at 153.4 mAh g^{-1} after the 70th cycle, i.e. up to 86.2% of the theoretical capacity, which is much higher than previously reported for $FePO_4$ as the cathode material of a sodium ion battery.[34] According to Fig. 10, the discharge-specific capacities of $FePO_4$ and the $FePO_4$/rGO composite were unstable during the initial cycles, and gradually stabilized after about 10 cycles. The specific-discharge capacity fluctuation during the initial cycles may be caused by the formation of micro-crystalline $NaFePO_4$ according to Fig. 6. This phenomenon has not been reported or mentioned in previous studies and the mechanism remains to be studied further. The results of the test clearly show that the discharge-specific capacity of the $FePO_4$/rGO composition, as a cathode material for SIBs, obviously improved when compared with the pure $FePO_4$ for SIBs.

Fig. 11 shows the capability of $FePO_4$/rGO and pure $FePO_4$ at different rates. The $FePO_4$/rGO shows a reversible capacity of 154.5 mAh g^{-1}, 151.6 mAh g^{-1},122.3 mAh g^{-1} and 100.6 mAh g^{-1} at 0.1C, 0.2C, 0.5C and 1C, respectively, which is much higher than pure $FePO_4$, which has a reversible capacity of 125.2 mAh g^{-1},104.3 mAh g^{-1},63.8 mAh g^{-1} and 37 mAh g^{-1} at 0.1C, 0.2C, 0.5C and 1C, respectively. The excellent rate capability of the $FePO_4$/rGO cathode material proves clearly that $FePO_4$/rGO is an ideal candidate for the cathode material of SIB.

Fig. 12 shows the electrochemical impedance spectra of $FePO_4$ and $FePO_4$/rGO, which is a semi-circle in the range of high to middle frequencies, and a straight line at low frequency. The semi-circle and straight line represent the process of charge transfer on an electrode surface, and the diffusion of sodium ions in the electrode, respectively. The corresponding equivalent circuit model is presented in Fig. 12 also. Rs represents electrolyte resistance, while CPE and Rct represent the constant phase element and charge transfer resistance, respectively. Zw corresponds to the sodium ion diffusion Warburg resistance.[51] According to the equivalent circuit, the result of fitting impedance parameters by Zview2 is shown in Table 1. Both kinds of material have a similar value of interface capacitance, which indicates that the interface structure of $FePO_4$ is unchanged by adding rGO. However, the value of Rct of $FePO_4$/rGO is 72.3 Ω, which is much lower than the Rct value of $FePO_4$ (199.3 Ω). Although both kinds of cathode material have a similar active material/electrolyte interface during the process of charging and discharging, the addition of rGO in $FePO_4$/rGO nanosheet composition makes electron transport much easier.

To explain the excellent electrochemical performance of $FePO_4$/rGO as a cathode material for SIBs, Fig. 13 presents a scheme to describe the transmission of electronic and sodium ions during the charge-discharge process. According to Fig. 13, the close adhesion between rGO and $FePO_4$ nanospheres could ensure that electrons transmit efficiently through the $FePO_4$/rGO interface. The rGO acts as a high-speed channel for electronic transfer. In addition, the nanoscale particle $FePO_4$ sphere, with a large specific surface area, can promote an active material/electrolyte interface reaction, and improve the speed of sodiation and desodiation during the charge and discharge process. The unique structure of the $FePO_4$/rGO nanosheet composition greatly enhances the efficient electronic and ionic conductivity, enabling a high specific capacity and high rate capability of this cathode material to be obtained.

4. Conclusion

A single-layer $FePO_4$/rGO nanosheet composition as a cathode material for SIBs has been synthesized by a micro-emulsion technique. The prepared micro-emulsion system makes the rGO distribution uniform, and the $FePO_4$ nanospheres grow successfully on the rGO by means of non-covalent bonds. The rGO in as-prepared $FePO_4$/rGO provides a high-speed pathway for electrons, and the $FePO_4$/electrolyte interface makes the sodium ions jump up and down easily. These features result in a high discharge-specific capacity and impressive rate capability. This work effectively improves the electrochemical performance of $FePO_4$ as a cathode material for sodium-ion batteries.

Acknowledgements

This work was carried out with the financial support of the Project of Shanghai Science & Technology Commission (13NM1401400), the Project of Ability Development of Shanghai Science & Technology Commission (09230501400), and the Research Foundation of the Ministry of Education (No.20502). We thank Proof-Reading-Service.com (http://www.proof-reading-service.com/) for its linguistic assistance during the preparation of this manuscript.

.

References

1. M. Armand and J. M. Tarascon, *Nature*, 2008, 451, 652-657.
2. B. Scrosati, *Electrochimica Acta*, 2000, 45, 2461-2466.
3. Y. Nishi, *Journal of Power Sources*, 2001, 100, 101-106.
4. M. R. Palacin, *Chemical Society Reviews*, 2009, 38, 2565-2575.
5. M. R. Hill, G. J. Wilson, L. Bourgeois and A. G. Pandolfo, *Energy & Environmental Science*, 2011, 4, 965-972.
6. B. Scrosati and J. Garche, *Journal of Power Sources*, 2010, 195, 2419-2430.
7. C. Wadia, P. Albertus and V. Srinivasan, *Journal of Power Sources*, 2011, 196, 1593-1598.
8. J. S. Huang, L. Yang, K. Y. Liu and Y. F. Tang, *Journal of Power Sources*, 2010, 195, 5013-5018.
9. K. T. Lee, T. N. Ramesh, F. Nan, G. Botton and L. F. Nazar, *Chemistry of Materials*, 2011, 23, 3593-3600.
10. S.-W. Kim, D.-H. Seo, X. Ma, G. Ceder and K. Kang, *Advanced Energy Materials*, 2012, 2, 710-721.
11. B. L. Ellis and L. F. Nazar, *Current Opinion in Solid State and Materials Science*, 2012, 16, 168-177.
12. X. Ma, H. Chen and G. Ceder, *Journal of The Electrochemical Society*, 2011, 158, A1307-A1312.
13. F. Sauvage, L. Laffont, J. M. Tarascon and E. Baudrin, *Inorganic Chemistry*, 2007, 46, 3289-3294.
14. V. Palomares, P. Serras, I. Villaluenga, K. B. Hueso, J. Carretero-Gonzalez and T. Rojo, *Energy & Environmental Science*, 2012, 5, 5884-5901.
15. E. Yoo, J. Kim, E. Hosono, H.-S. Zhou, T. Kudo and I. Honma, *Nano Letters*, 2008, 8, 2277-2282.
16. A. K. Padhi, K. S. Nanjundaswamy and J. B. Goodenough, *Journal of The Electrochemical Society*, 1997, 144, 1188-1194.
17. J. L. Allen, T. R. Jow and J. Wolfenstine, *J Solid State Electrochem*, 2008, 12, 1031-1033.
18. S. W. Oh, S.-T. Myung, S.-M. Oh, K. H. Oh, K. Amine, B. Scrosati and Y.-K. Sun, *Advanced Materials*, 2010, 22, 4842-4845.
19. F. F. C. Bazito and R. M. Torresi, *Journal of the Brazilian Chemical Society*, 2006, 17, 627-642.
20. S. M. Zhang, J. X. Zhang, S. J. Xu, X. J. Yuan and B. C. He, *Electrochimica Acta*, 2013, 88, 287-293.
21. X. Yang, S. M. Zhang, J. X. Zhang, *Functional Materials Letters*, 2011, 4, 4, 323-326.
22. S.-Y. Chung, J. T. Bloking and Y.-M. Chiang, *Nat Mater*, 2002, 1, 123-128.
23. X.-F. Zhang, K.-X. Wang, X. Wei and J.-S. Chen, *Chemistry of Materials*, 2011, 23, 5290-5292.
24. S. Xu, S. Zhang, J. Zhang, T. Tan and Y. Liu, *Journal of Materials Chemistry*

A, 2014, 2, 7221-7228.

25. C. Berger, Z. Song, X. Li, X. Wu, N. Brown, C. Naud, D. Mayou, T. Li, J. Hass, A. N. Marchenkov, E. H. Conrad, P. N. First and W. A. de Heer, *Science*, 2006, 312, 1191-1196.

26. K. S. Novoselov, A. K. Geim, S. V. Morozov, D. Jiang, Y. Zhang, S. V. Dubonos, I. V. Grigorieva and A. A. Firsov, *Science*, 2004, 306, 666-669.

27. S. Yang, X. Feng and K. Müllen, *Advanced Materials*, 2011, 23, 3575-3579.

28. J. Zhou, J. Wang, L. Zuin, T. Regier, Y. Hu, H. Wang, Y. Liang, J. Maley, R. Sammynaiken and H. Dai, *Physical Chemistry Chemical Physics*, 2012, 14, 9578-9581.

29. Y. Zhu, S. Murali, W. Cai, X. Li, J. W. Suk, J. R. Potts and R. S. Ruoff, *Advanced Materials*, 2010, 22, 3906-3924.

30. H. A. Cha, H. M. Jeong and J. K. Kang, *Journal of Materials Chemistry A*, 2014, 2, 5182-5186.

31. Y. Liu, Y. Zhao, L. Jiao and J. Chen, *Journal of Materials Chemistry A*, 2014, 2, 13109-13115.

32. H. Geng, S. F. Kong and Y. Wang, *Journal of Materials Chemistry A*, 2014, 2, 15152-15158.

33. Q. Fan, L. Lei, X. Xu, G. Yin and Y. Sun, *Journal of Power Sources*, 2014, 257, 65-69.

34. Q. Fan, L. Lei, G. Yin, Y. Chen and Y. Sun, *Electrochemistry Communications*, 2014, 38, 120-123.

35. W. Gu, W. Zhang, X. Li, H. Zhu, J. Wei, Z. Li, Q. Shu, C. Wang, K. Wang, W. Shen, F. Kang and D. Wu, *Journal of Materials Chemistry*, 2009, 19, 3367-3369.

36. L. Zhu, X. Zhao, Y. Li, X. Yu, C. Li and Q. Zhang, *Materials Chemistry and Physics*, 2013, 137, 984-990.

37. D. C. Marcano, D. V. Kosynkin, J. M. Berlin, A. Sinitskii, Z. Sun, A. Slesarev, L. B. Alemany, W. Lu and J. M. Tour, *ACS Nano*, 2010, 4, 4806-4814.

38. S. Stankovich, R. D. Piner, S. T. Nguyen and R. S. Ruoff, *Carbon*, 2006, 44, 3342-3347.

39. K. S. Novoselov, A. K. Geim, S. V. Morozov, D. Jiang, M. I. Katsnelson, I. V. Grigorieva, S. V. Dubonos and A. A. Firsov, *Nature*, 2005, 438, 197-200.

40. H. Hiura, T. W. Ebbesen, K. Tanigaki and H. Takahashi, *Chemical Physics Letters*, 1993, 202, 509-512.

41. J. C. Charlier, P. C. Eklund, J. Zhu and A. C. Ferrari, in *Carbon Nanotubes*, eds. A. Jorio, G. Dresselhaus and M. Dresselhaus, Springer Berlin Heidelberg, 2008, vol. 111, ch. 21, pp. 673-709.

42. G. Wang, J. Yang, J. Park, X. Gou, B. Wang, H. Liu and J. Yao, *The Journal of Physical Chemistry C*, 2008, 112, 8192-8195.

43. A. C. Ferrari, J. C. Meyer, V. Scardaci, C. Casiraghi, M. Lazzeri, F. Mauri, S. Piscanec, D. Jiang, K. S. Novoselov, S. Roth and A. K. Geim, *Physical Review Letters*, 2006, 97, 187401.

44. J. C. Meyer, A. K. Geim, M. I. Katsnelson, K. S. Novoselov, T. J. Booth and S. Roth, *Nature*, 2007, 446, 60-63.

45. J. N. Bridson, S. E. Quinlan and P. R. Tremaine, *Chemistry of Materials*, 1998, 10, 763-768.

46. V. Mathew, S. Kim, J. Kang, J. Gim, J. Song, J. P. Baboo, W. Park, D. Ahn, J. Han, L. Gu, Y. Wang, Y.-S. Hu, Y.-K. Sun and J. Kim, *NPG Asia Mater*, 2014, 6, e138.

47. Y. Zhu, Y. Xu, Y. Liu, C. Luo and C. Wang, *Nanoscale*, 2013, 5, 780-787.

48. Y. Fang, L. Xiao, J. Qian, X. Ai, H. Yang and Y. Cao, *Nano Letters*, 2014, 14, 3539-3543.

49. Y. Liu, Y. Xu, X. Han, C. Pellegrinelli, Y. Zhu, H. Zhu, J. Wan, A. C. Chung, O. Vaaland, C. Wang and L. Hu, *Nano Letters*, 2012, 12, 5664-5668.

50. D. Hamani, M. Ati, J.-M. Tarascon and P. Rozier, *Electrochemistry Communications*, 2011, 13, 938-941.

51. S. P. Ong, V. L. Chevrier, G. Hautier, A. Jain, C. Moore, S. Kim, X. Ma and G. Ceder, *Energy & Environmental Science*, 2011, 4, 3680-3688.

Table and figures

Table 1 Fitted electrochemical impedance spectra parameters of $FePO_4$/rGO composite and $FePO_4$.

Sample	$FePO_4$/rGO	$FePO_4$
Rs(Ω)	26.66	22.81
CPE-T	0.00015287	0.00012728
CPE-P	0.50338	0.57954
Rct(Ω)	72.3	199.3

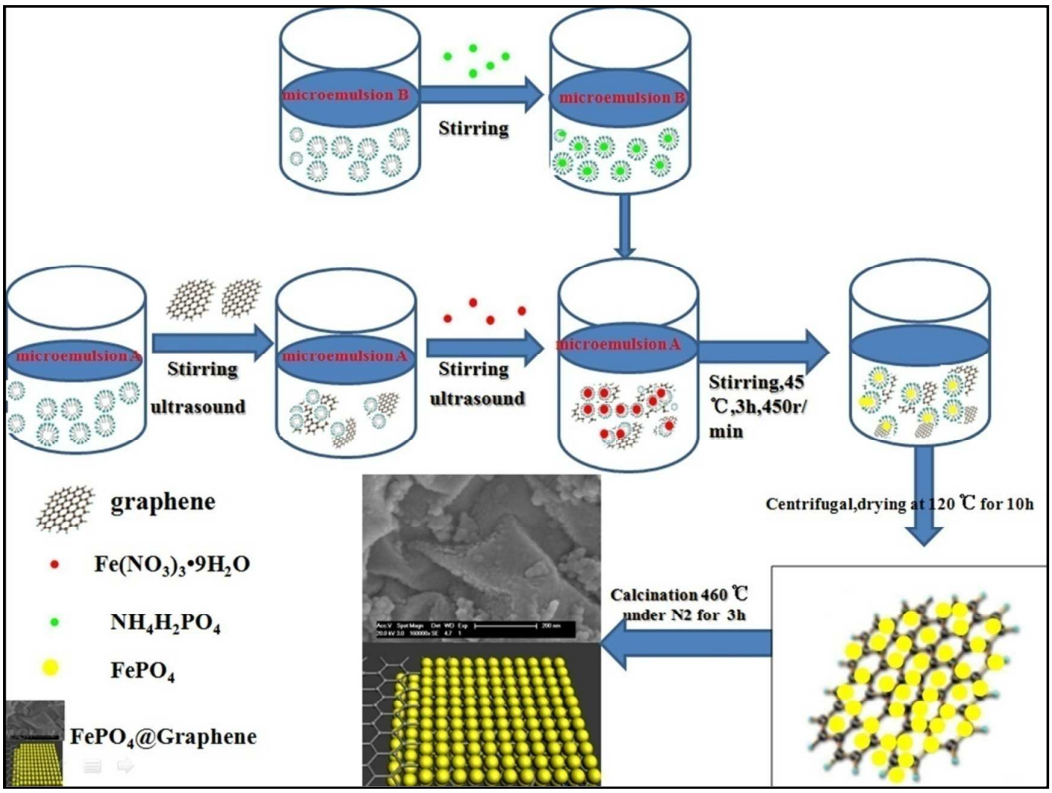

Fig. 1. Synthesis scheme of the $FePO_4$@rGO composite by a micro-emulsion technique

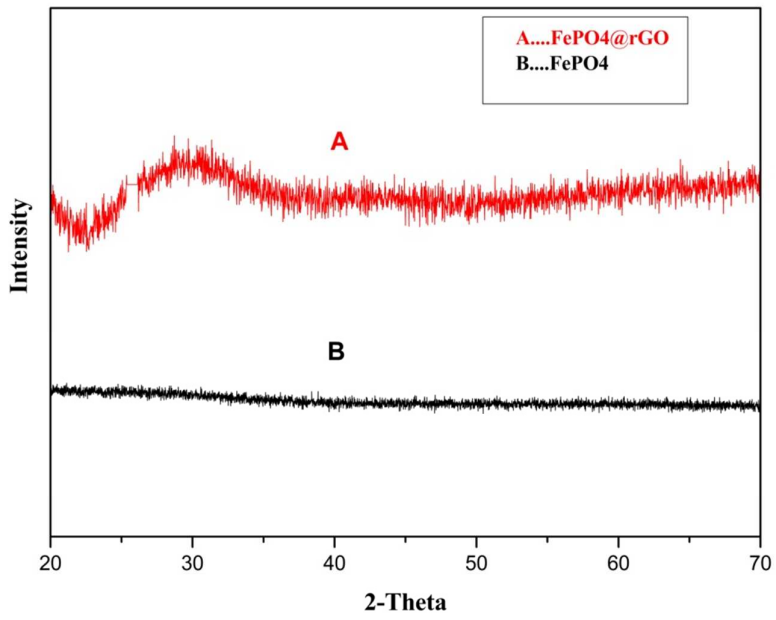

Fig. 2. XRD patterns of $FePO_4$ and $FePO_4$/rGO composite

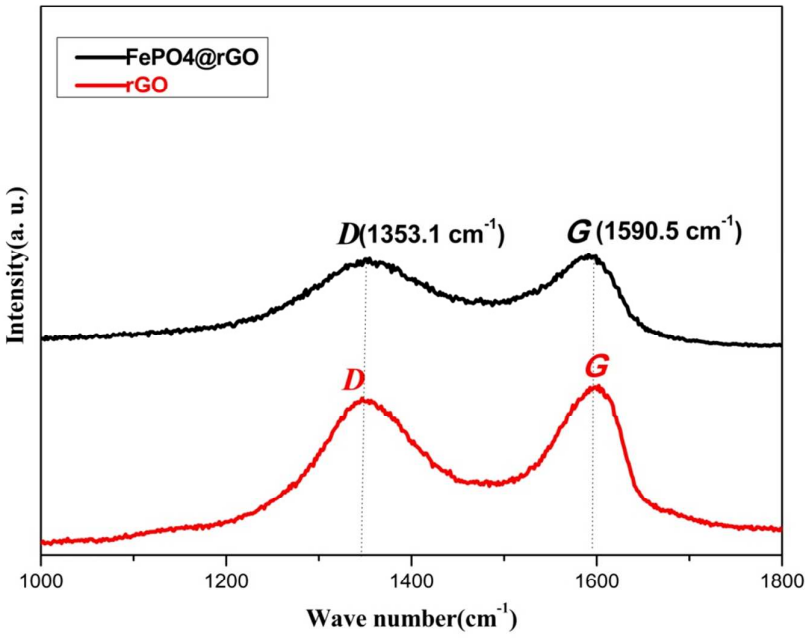

Fig. 3. Raman spectra of rGO and $FePO_4$/rGO composite

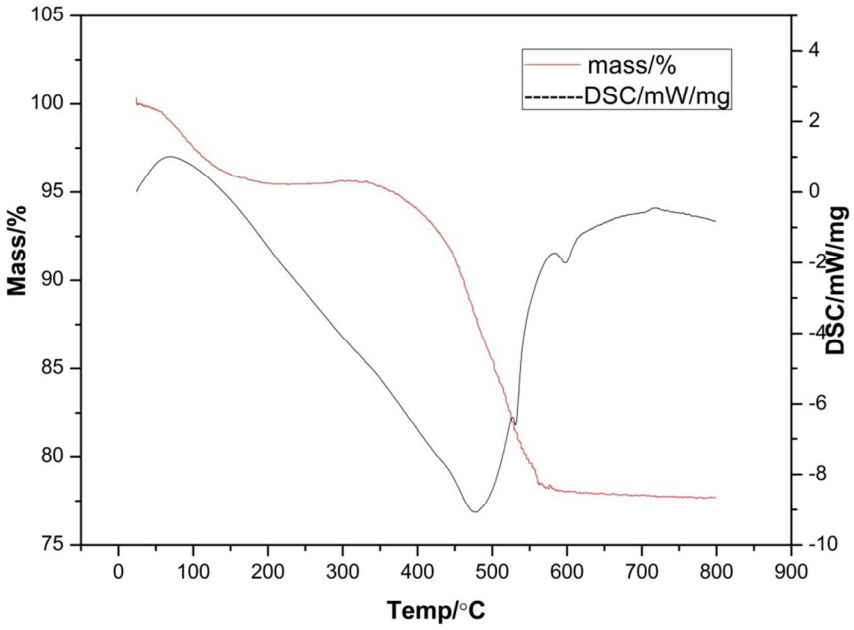

Fig. 4. TGA-DSC of $FePO_4$/rGO composite

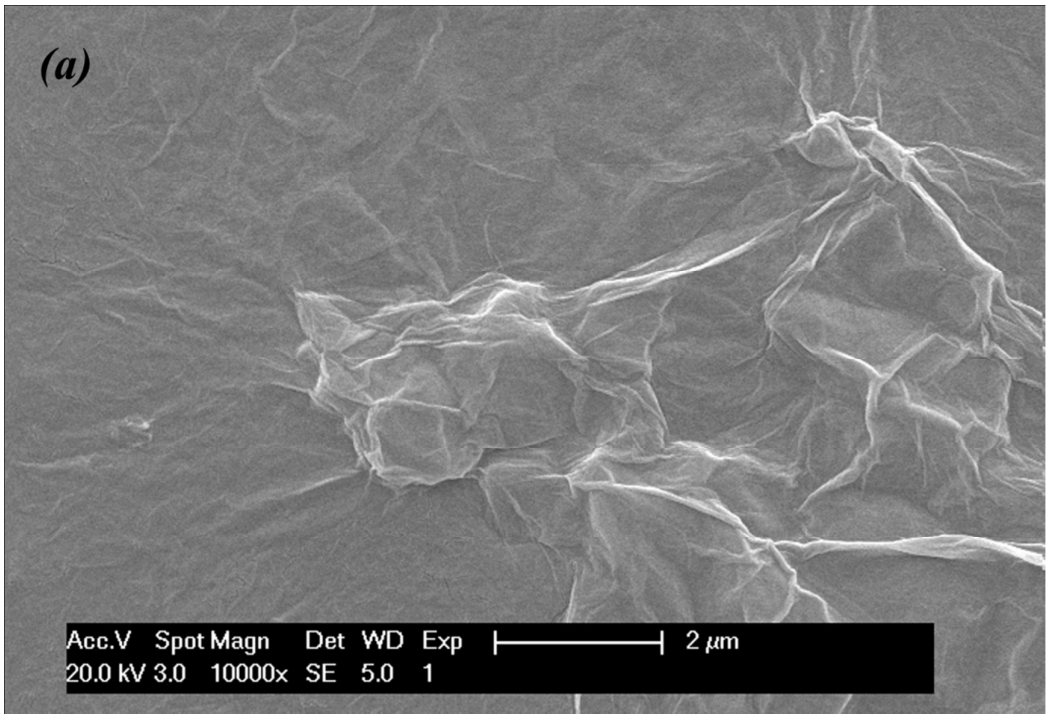

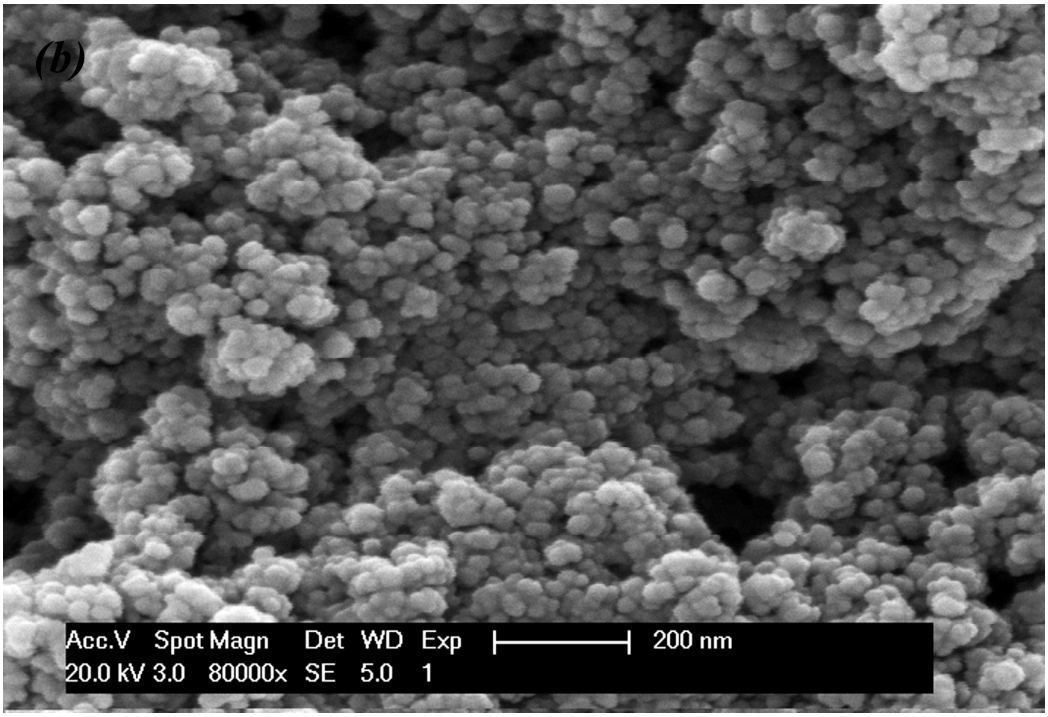

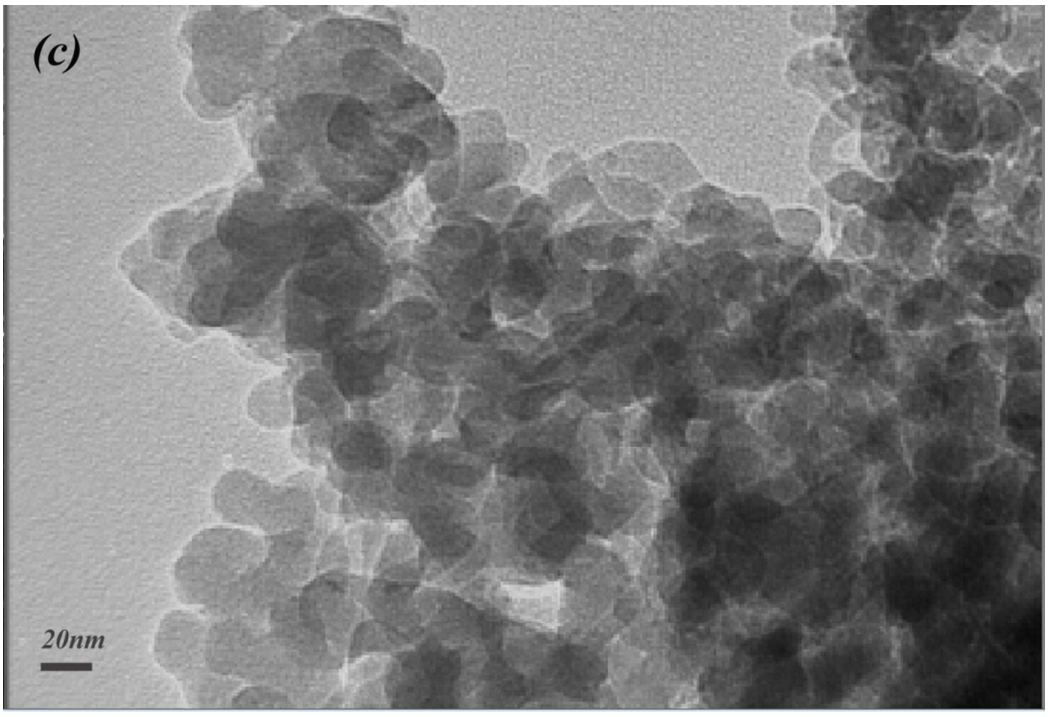

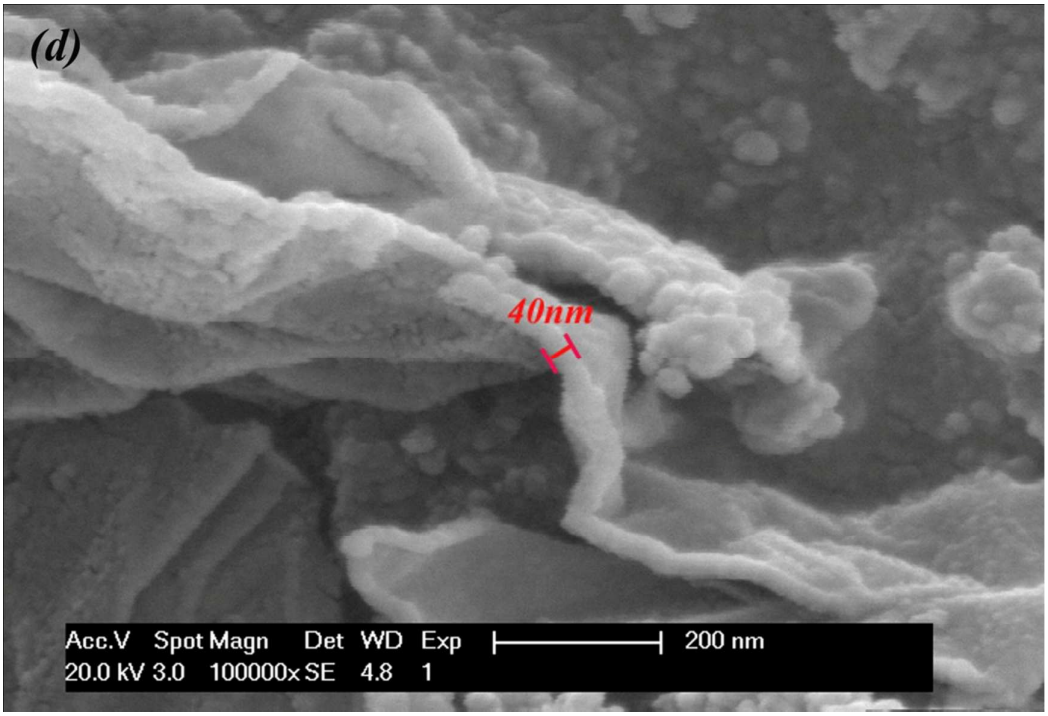

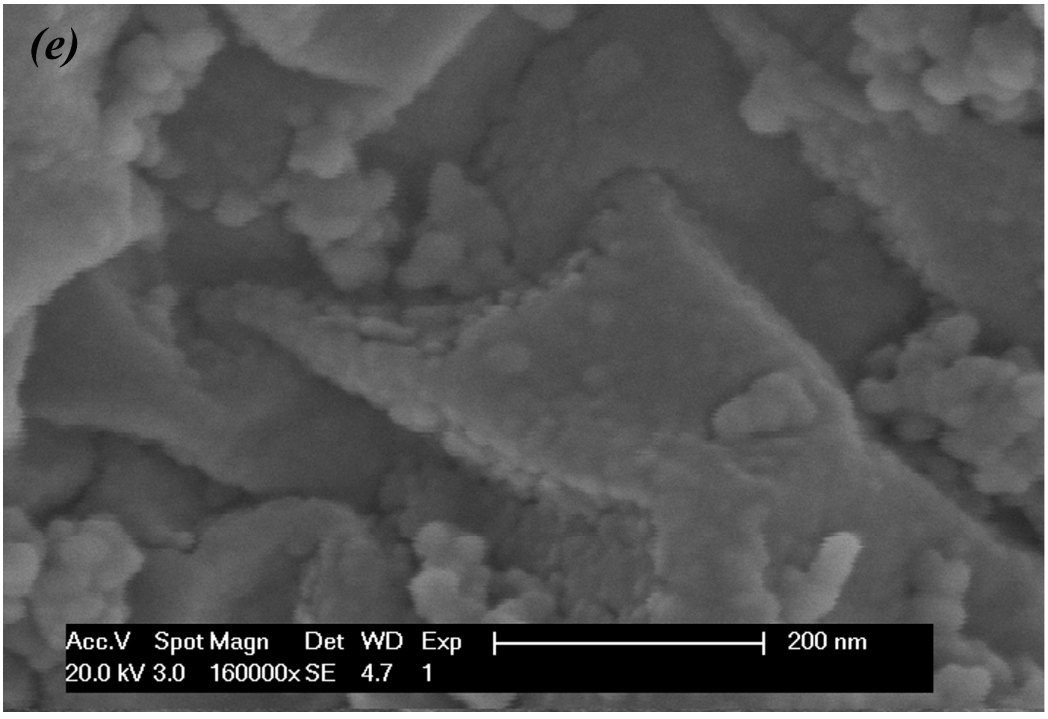

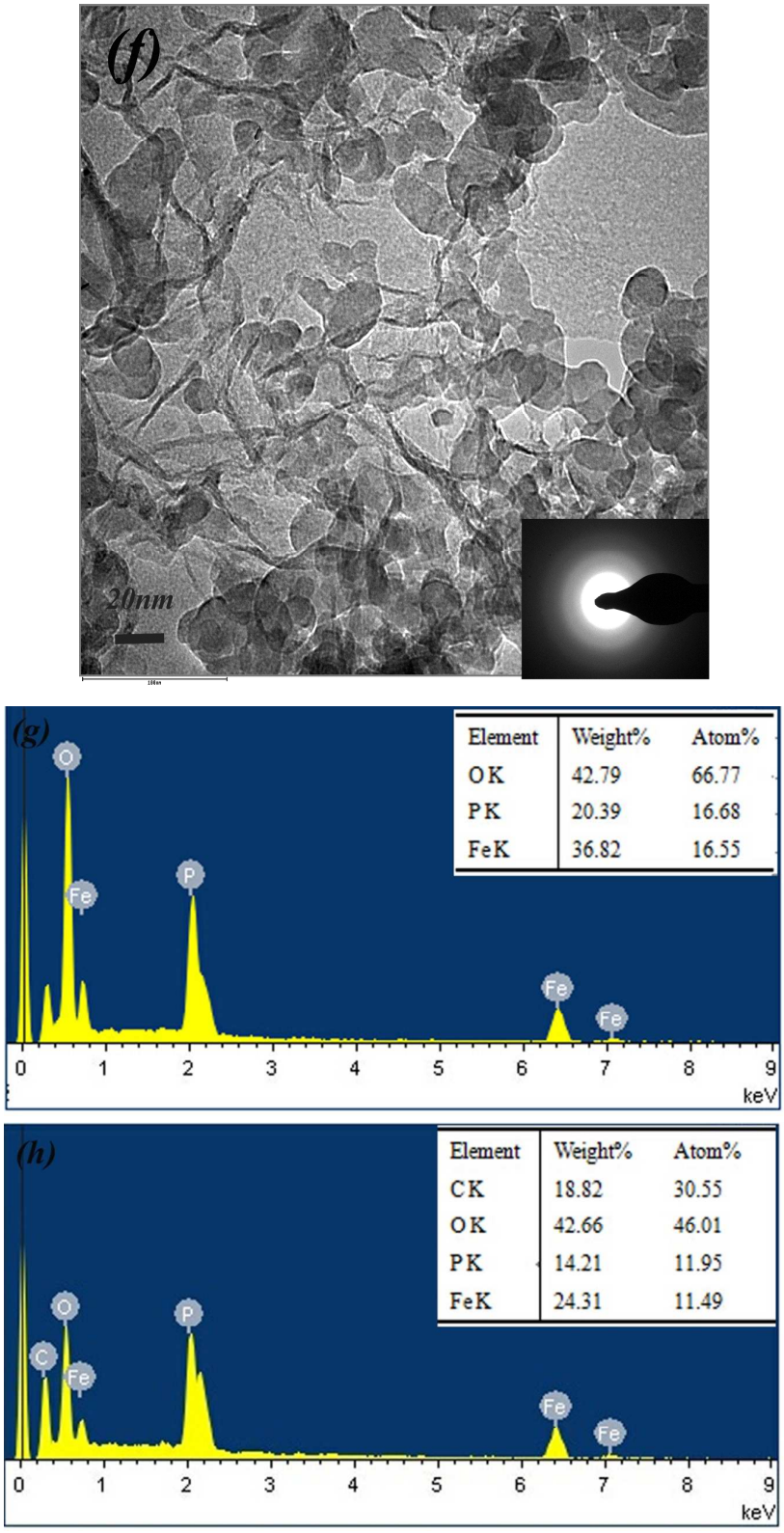

Fig. 5. (a) SEM images of rGO; (b, c) SEM and TEM images of $FePO_4$; (d, e, f) SEM and TEM images of $FePO_4$/rGO composite, (g, h) EDS of $FePO_4$

and $FePO_4$/rGO.

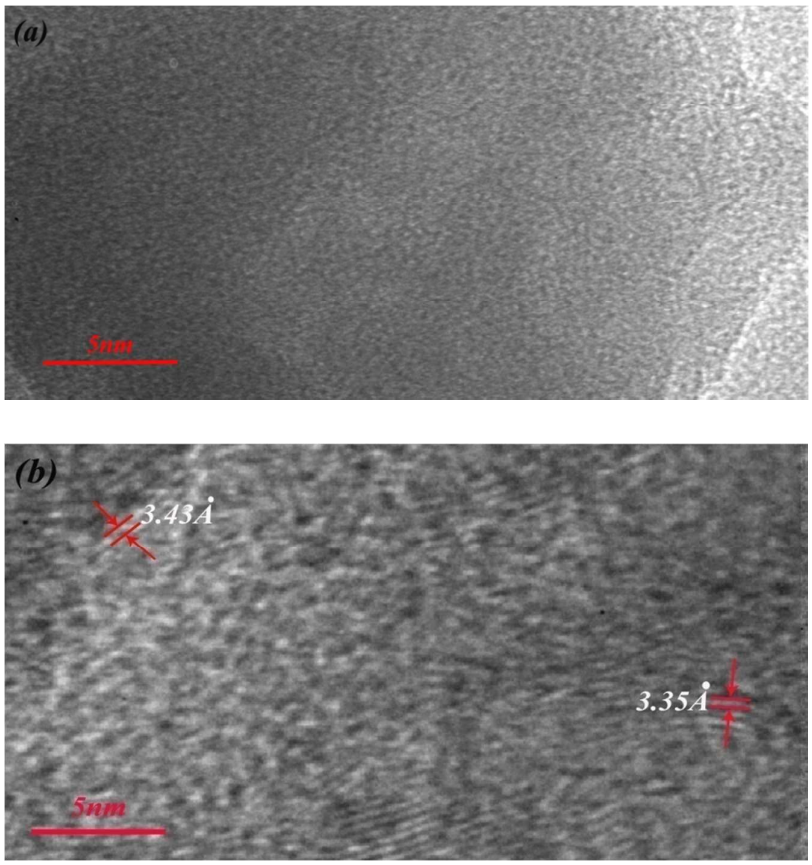

Fig. 6. (a, b) high-resolution TEM images of $FePO_4$/rGO before and after sodiation

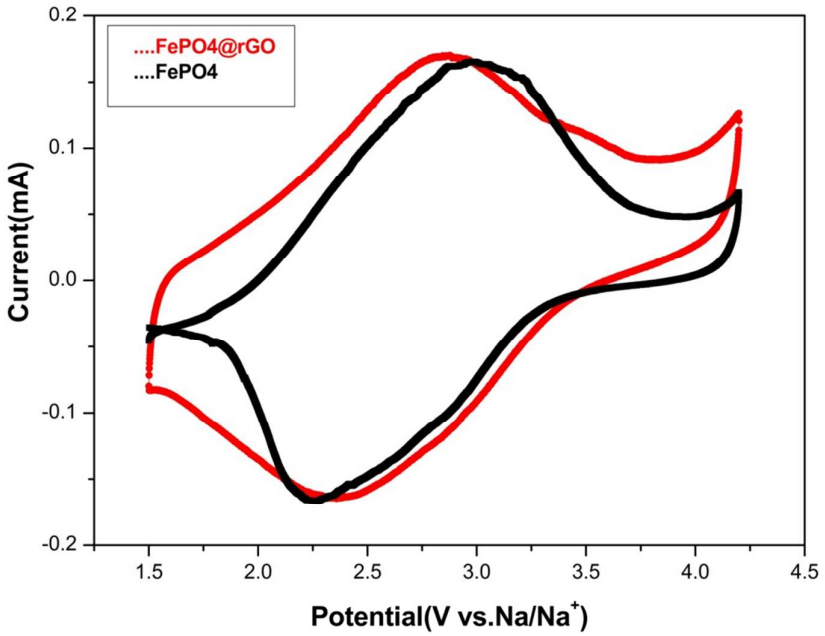

Fig. 7. CV curve conducted at a scan rate of 0.05 mV s^{-1} (voltage window 1.5–4.2V) for $FePO_4$ and $FePO_4$/rGO composite.

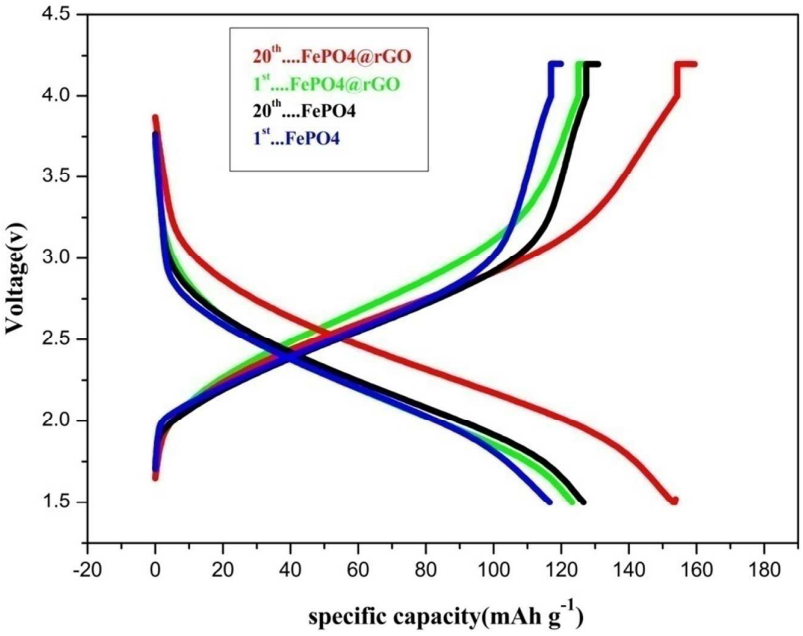

Fig. 8. Galvanostatic discharge/charge profiles at 1st and 20th cycles for $FePO_4$ and $FePO_4$/rGO composite at 0.1C

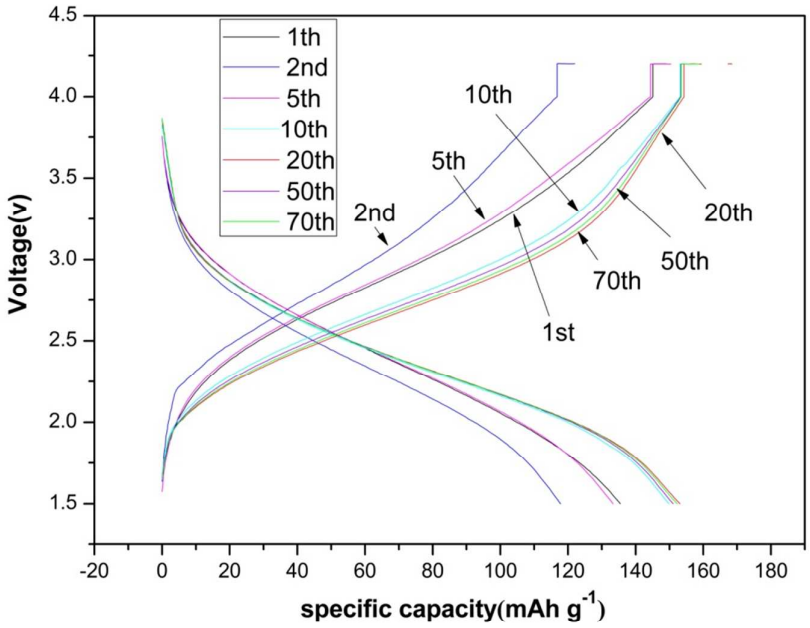

Fig. 9. Galvanostatic discharge/charge profiles at 1^{st}, 2^{nd}, 5^{th}, 10^{th}, 20^{th}, 50^{th}, and 70^{th} cycles for $FePO_4$/rGO composite at 0.1C

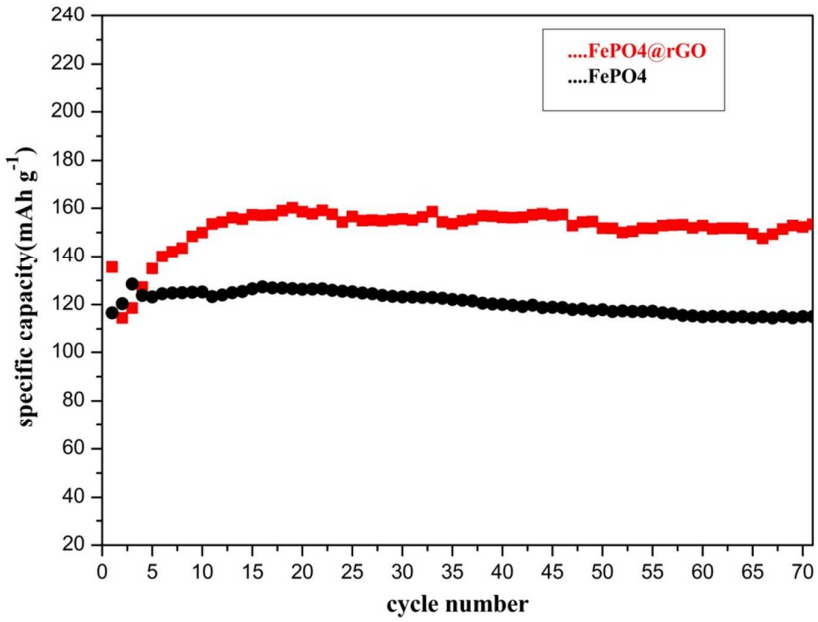

Fig. 10. Discharge-specific capacity versus cycle number for $FePO_4$ and the $FePO_4$/rGO composite at 0.1C.

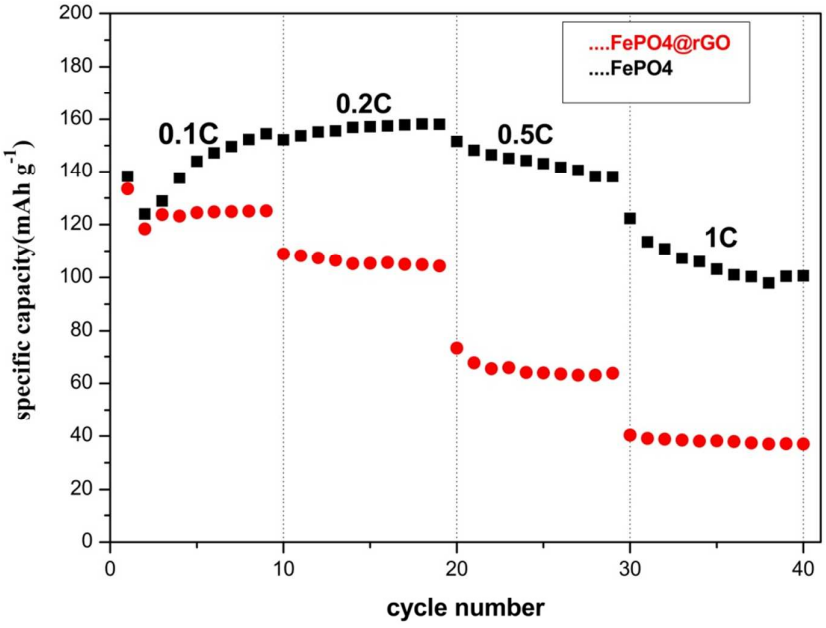

Fig. 11. Rate capability curves of $FePO_4$ and the $FePO_4$/rGO composite

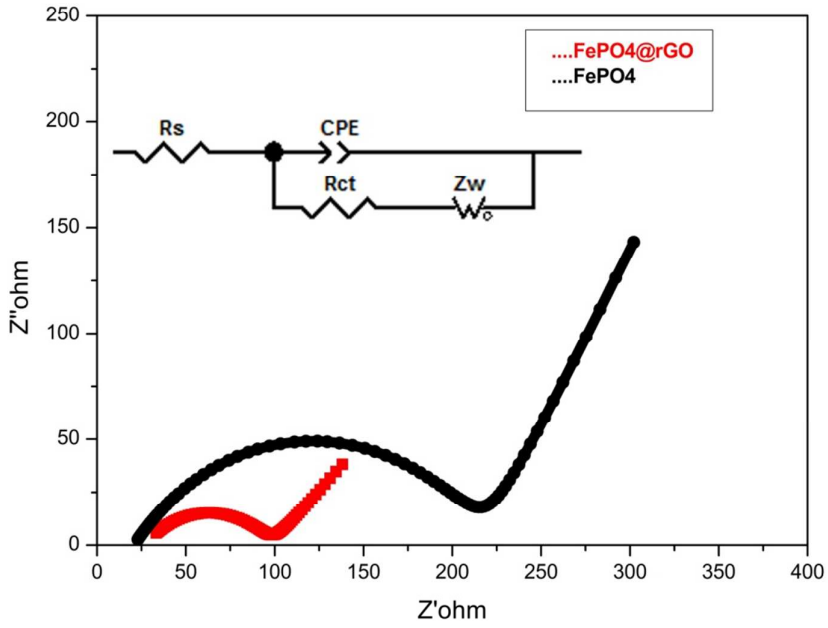

Fig. 12. Electrochemical impedance spectra and equivalent circuit of $FePO_4$ and $FePO_4$/rGO composite.

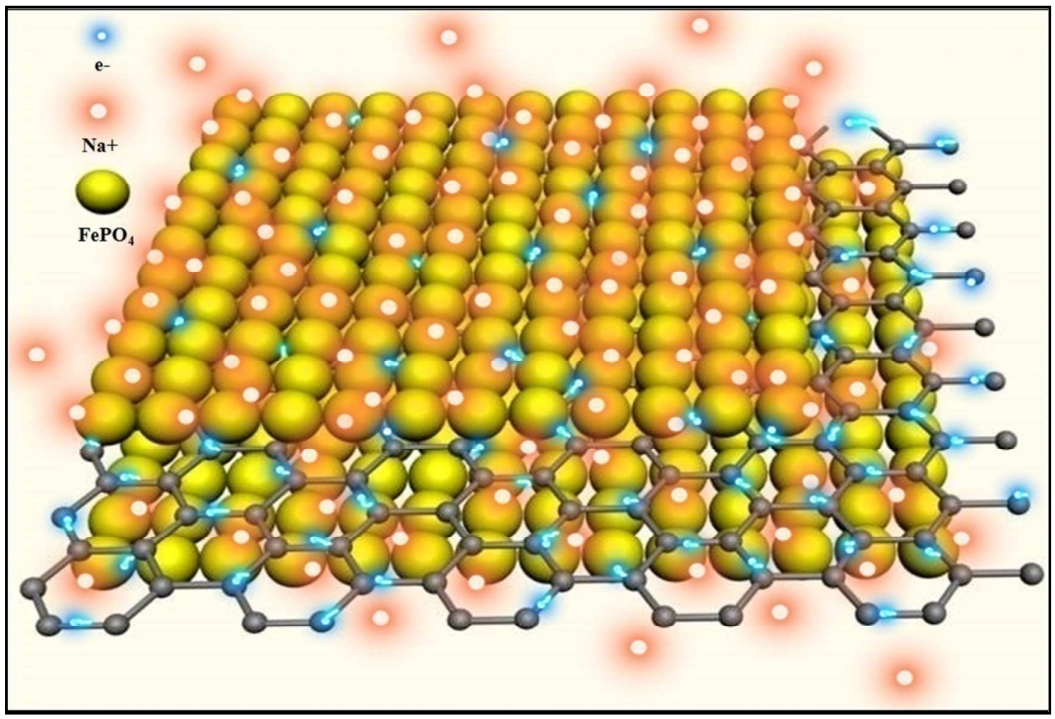

Fig. 13. Scheme of the transport processes of electrons and sodium ions in the $FePO_4$/rGO composite during charging and discharging

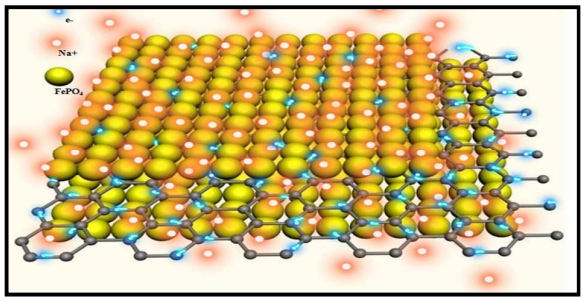

The direct growth of $FePO_4$/reduced graphene oxide nanosheet composite cathode material for sodium-ion batteries via a micro-emulsion technique, which exhibits excellent electrochemical performance.